CONF-9507176--1
SAND95-1385C

Cryogenic Design of the Liquid Helium Experiment "Critical Dynamics in Microgravity"

W. A. Moeur[1], M. J. Adriaans[2], S. T. P. Boyd[2], D. M. Strayer[3], and R. V. Duncan[2]

[1] University of New Mexico, Albuquerque, New Mexico, USA
[2] Sandia National Laboratories, Albuquerque, New Mexico, USA
[3] Jet Propulsion Laboratory, Pasadena, California, USA

ABSTRACT

Although many well controlled experiments have been conducted to measure the static properties of systems near criticality, few experiments have explored the transport properties in systems driven far away from equilibrium as a phase transition occurs. The cryogenic design of an experiment to study the dynamic aspect of critical phenomena is reported here. Measurements of the thermal gradient across the superfluid (He II) - normal fluid (He I) interface in helium under microgravity conditions will be performed as a heat flux holds the system away from equilibrium. New technologies are under development for this experiment, which is in the definition phase for a space shuttle flight.

KEYWORDS: superfluid helium, lambda transition, microgravity, critical phenomena

I. INTRODUCTION

Although static critical phenomena are relatively well studied, very little is known about transport properties through criticality in general. This is unfortunate, since in nature virtually all phase transitions occur while a system is driven far from equilibrium. Hence, a first-principles understanding of critical phenomena under highly nonequilibrium conditions is of fundamental importance to explain real world processes. In transport measurements, a system is held out of equilibrium and maintained in a well controlled steady-state condition. In our experiments, thermal gradients very near the normal fluid superfluid interface (He I - He II) are measured with sub-nanokelvin resolution [1]. Under the influence of gravity, the He I - He II interface may be positioned (or maintained) by adjusting (or regulating) the temperature of the superfluid component. In the low heat flux limit of our experiments this superfluid component is isothermal. In Earth orbit, theory predicts the interface should be stabilized by the heat

flux [2]; however once in Earth orbit, these experiments do not depend upon this predicted stabilization in order to obtain data.

The superfluid transition in pure liquid ^{4}He provides an excellent opportunity to test modern theories of second-order phase transitions. The ^{4}He sample is ultra-pure; the ^{3}He isotope, which may be purified to a few parts in 10^{12} presents the only impurity [3,4]. Unlike solid systems which, even in the high-purity limit support vacancies and grain boundaries, ^{4}He near its superfluid transition is homogeneous. According to the Psi Theory [5], superfluid helium can be described by a two-component order parameter, often referred to as the "wavefunction of the condensate." In most critical phenomena studies, the field conjugate to the order parameter creates a rounding of the transition. The ^{4}He superfluid transition is unusual in that the conjugate field is not physical [5], and hence the superfluid transition in ^{4}He remains sharp. Since the superfluid transition temperature, T_λ, varies with pressure (-113 bar/K near saturated vapor pressure [6]), T_λ varies with height along a column of ^{4}He subject to gravity. To avoid gravitationally induced sample pressure gradients, precise heat capacity measurements in bulk ^{4}He were conducted in the Lambda Point Experiment (LPE) in Earth orbit in late 1992 [7]. Another heat capacity experiment, the Confined Helium Experiment (CHeX), performed in a confined geometry where finite-size effects are measurable, is now under development for space deployment in 1997 [8]. Our thermal conductivity experiment, Critical Dynamics in Microgravity (DYNAMX), is tentatively planned for flight aboard the Space Shuttle in the year 2000.

This paper documents the cryogenic apparatus and procedures which are currently used in the prototype instrument to obtain data on Earth. Modifications of this apparatus for the flight version, together with the intended adjustment of the data acquisition once in Earth orbit, are also discussed. The flight instrument is being designed to fly within the Low-Temperature Research Facility (LTRF) of the Jet Propulsion Laboratory (JPL). The LTRF platform has already flown twice in Earth orbit and is scheduled to fly once again prior to the launch of DYNAMX.

II. BACKGROUND

Recently, dynamic renormalization group theory has been applied to predict the thermal profile through a He I - He II interface subjected to a heat flux Q [9]. This theory predicts that the effective thermal conductivity of the He I does not diverge, but rather approaches a finite value which strongly depends on Q as the temperature approaches T_λ. If this prediction of a non-ohmic thermal conductivity is verified experimentally, the experiment will constitute the first study of how a system's linear response to an external heat flux breaks down near criticality. This theory [9] and another theory based primarily on a dynamic scaling approach [2] predict that the width of the He I - He II interface decreases with increasing heat flux as Q^{-x}, where $x \sim 0.5$. Since this interfacial width is essentially the correlation length, ξ, these measurements would provide the first measurement of how the correlation length in a system at criticality varies with the non-equilibrium parameter (here the constant heat flux).

Both the renormalization group theory [9,10] and the dynamic scaling theory [2] predict a depression of the superfluid transition temperature by the heat flux. This effect has been observed experimentally [11], and small discrepancies exist between the theory [9] and the experimental results. Below $T_\lambda(Q)$, at small Q, the helium is isothermal [11]. The nature of the thermal profile within the helium at temperatures in the range $T_\lambda(Q) < T < T_\lambda(Q=0)$ is still unknown. Its determination remains an exciting challenge.

So far, measurements of bulk helium properties, especially close to the superfluid transition temperature where boundary effects diverge, are plagued by the presence of the endplates in the experimental cell. The thermal resistance, also known as the Kapitza resistance, between the superfluid helium and a solid (usually metal) endplate has been observed to be weakly singular at T_λ and, for temperatures near T_λ to exhibit a sudden onset to a strongly non-ohmic (Q-dependent) behavior which saturates to a Q-independent value for temperatures approaching T_λ [12,13,14]. Only the origin of the weak Q-independent singularity has been explained theoretically [15]. Although it is much more difficult to measure the thermal boundary resistance between normal fluid helium and the endplate, initial studies [15,16,17] suggest that a singular (and possibly Q-dependent) boundary resistance exists on this side of the transition as well. The depression of the superfluid transition temperature with a heat flux was measured

with the He I - He II interface forming at the bottom endplate of the cell [11]. Future measurements will measure $T_\lambda(Q)$ when the interface reaches a sidewall platform, thereby minimizing endplate effects. Since endplate effects (which fall off exponentially with the bulk correlation length ξ) become pronounced at much larger reduced temperatures than do the nonlinear bulk effects, the endplate effects are predicted to be more than an order of magnitude larger than the predicted bulk nonlinear helium properties [9] under study. To make at least a 1% measurement of these bulk nonlinear properties, thermometers must be located at a distance of at least 10ξ from either cell endplate. A reduced temperature of $t \sim 10^{-9}$, where $t = (T-T_\lambda)/T_\lambda$, may be realistically maintained in our experiment. At this reduced temperature, $\xi \sim 0.22$ mm, and the 10ξ rule mandates that the measurements be made at least 2.2 mm from the endplates.

Experiments performed under gravity have qualitatively (yet not quantitatively) confirmed the existence of the nonlinear thermal conductivity region predicted by theory [18]. These measurements were made in small cells to avoid convection. Hence, in these measurements, it was very difficult to conclusively separate the singular boundary effects from the nonlinear bulk thermal conductivity effects. Since only the helium very near the cold endplate of the cell was in the nonlinear region, most of the remaining helium was in the linear region due to the existence of the thermal gradient across the helium layer. In order to observe other predictions from theory, such as the Q-dependence of the interface thickness (and hence of ξ at t=0), it is necessary to measure the actual thermal profile near and through the He I - He II interface with the highest possible thermal and spatial resolution. Only microgravity conditions sustained over many days will permit these effects to be conclusively studied experimentally.

One concern, the need to avoid pressure-induced sample nonuniformity, motivates the microgravity requirements for the static (heat capacity) experiments [7,8]. For $Q \sim 0.1$ μW/cm^2, this same concern applies to the dynamic measurements. At these small values of Q, the pressure-induced variation in T_λ pushes the system away from criticality more than does the resulting thermal gradient in the normal fluid. At the opposite extreme, values of $Q > .3$ μW/cm^2 create such a large thermal gradient in a cell of approximately 7 mm that convection is produced in the normal fluid on Earth [19]. Hence, an earth-based experiment would be unable to measure the diverging diffusive thermal conductivity of the normal state. Performing these experiments in microgravity also permits using larger values of Q. Finally, the width of

the He I - He II interface has been predicted to vary as Q^x, with $x \sim 0.5$ [2,9]. Under gravity, however, this variation cannot be directly measured since gravity reduces the initial width of the $Q = 0$ interface to only a few tens of micrometers. In orbit, the initial $Q = 0$ width has been predicted [8] to increase to about one millimeter, making its measurement practical.

III. APPARATUS

General Probe Design

The probe, which is placed inside a vacuum can machined from a single piece of aluminum, consists of five actively temperature-regulated stages thermally connected to each other through known thermal impedances (Figure 1). The uppermost and coldest stage is the 1 K stage which is strongly connected to the 1 K refrigerator and is not regulated. Four RF SQUIDs attach to their own, separately regulated, copper platform. The temperature of the SQUID stage can be controlled to help prevent stray heat from affecting the high resolution thermometers. The second stage from the top is the isothermal platform which is regulated with a germanium resistance thermometer (GRT). The final stage, before the experimental platform, is the shield stage. The shield stage surrounds the experimental platform to provide isolation from blackbody radiation from the uncontrolled 4 K bath. The shield stage can be regulated with either a GRT bridge or a paramagnetic salt thermometer (PST).

The experimental cell has heaters attached to both its top and bottom end plates. The top heater works in conjunction with either the GRT mounted on top of the cell or the top PST to provide temperature regulation. The bottom heater provides the heat flux for the measurements.

All electrical wiring, except the triaxial lines of the RF SQUIDs, are brought in twisted pairs to a 55-pin hermetic glass-metal connector. This connector is soldered into a brass flange which is in turn bolted to the vacuum can lid using an indium seal. The RF SQUID signals are brought through the superconducting SQUID housings along rigid stainless steel coaxial lines that are themselves enclosed in stainless steel sheaths to form a triaxial line. This configuration isolates the VHF SQUID bias ground from the low-level signal ground of the cryostat. The triaxial symmetry is broken, however, at the feed-through to the helium bath. Here, the two inner conductors are separated and each is fed through its own glass-

metal hermetic insulated pin. Like the 55-pin connector these single pins must be soldered in place using a low temperature solder, and cannot withstand much lateral stress before losing their hermeticity.

The system is cooled below the boiling point of helium by a 1 K refrigerator. The 1 K refrigerator consists of a small OFHC copper chamber which is pumped via a 2.5 cm diameter line with a 0.65 cubic-meter-per-minute direct-drive pump. The pump pulls liquid helium from the bath into the chamber through a 5 μm filter and a 10 cm length of 0.15 mm diameter stainless steel capillary with a 0.14 mm diameter wire inserted into it. This arrangement of wire and capillary provides a measured impedance of $6x10^{11}$ cm^{-3} and a cooling power of about 9 mW.

To fill the experimental cell, ultra-high purity ^4He [3] is passed through a liquid nitrogen cold trap and down through the main liquid helium bath via a 0.5 mm diameter stainless steel capillary to the vacuum can. After passing through the vacuum can feed-through the capillary is heat sunk to the 1 K stage. The heat sink removes some heat from the helium before the liquid reaches the cryogenic valve which is thermally attached to the shield stage. After passing through the valve, the helium fills both the cell and a vapor pressure pot. The vapor pressure pot rests on the shield stage, but is thermally connected to the cell. Hence, the vapor pressure pot is isothermal with the experimental cell. The pressure of the helium sample must be maintained to within about 1 mPa to assure that pressure fluctuations do not create any more than a 0.1 nK fluctuation in T_λ. A liquid-vapor interface must exist in this vapor pressure pot to maintain saturated vapor pressure conditions in the liquid. In flight, the vapor pressure pot will be replaced by a chamber which creates a vapor pressure bubble out of the cell's heat path. The vapor pressure bubble must be greater than one millimeter in radius to avoid pressure corrections from the liquid-vapor surface tension.

High Resolution Thermometry

High resolution temperature measurement and control is accomplished in this experiment by using paramagnetic salt thermometers. The thermometers are similar in design to those used in previous experiments near the lambda transition [1]. PSTs work by taking advantage of the temperature dependent magnetic susceptibility of the material used as the sensing element. When the paramagnetic material is placed in an external magnetic field it develops a magnetization proportional to its susceptibility. A change

in the temperature of the salt therefore causes a change in its magnetization. A superconducting pick-up coil, wound around the salt, maintains a constant magnetic flux through itself by changing the current in the loop to counter the changing magnetic field of the salt. The changes in the current are then measured by an RF SQUID.

Two slightly different types of PSTs have been installed in the DYNAMX cryostat. Both are solenoidal and use the paramagnetic salt copper ammonium bromide (CAB). The sensing element used in the first type of thermometer is made up of multiple crystals of CAB grown around an array of copper wires which provides for thermal contact. The sensing element is placed inside a sapphire post which is attached to a high purity (>99.999%), annealed aluminum rod. The superconducting pick-up coil is wrapped around the outside of the sapphire holder. The second type of thermometer is made from a packed powder of CAB. Copper wires are imbedded in the powder for thermal contact. A beryllium-copper cylinder is used to house the packed CAB and its contact wires, and the pick-up coil is wrapped around the outside of the cylinder. The cylinder is then sealed and attached to an annealed copper rod. Both thermometers are placed inside superconducting niobium flux tubes which trap a constant magnetic field of about one kilogauss.

A third type of PST is currently under investigation. Due to the long cylindrical shape of the current thermometers, shuttle launch load vibrations could significantly heat the experiment [20]. To keep the flux tubes cooled and superconducting through the launch, a ^{3}He exchange gas must be introduced into the cryostat's vacuum space. Up to two days, during which no data can be collected, will be required to pump this exchange gas out to space. Changing the geometry of the PST to a toroid may lower the vibration-induced heat load and thereby eliminate the need for an exchange gas. A toroidal PST has been built and read out with an inductive bridge [21]. Work is in progress to build and test the toroidal thermometer with a SQUID readout. The sensing element of the toroidal thermometer is a packed powder annulus of CAB with an inner diameter of 1.3 cm, an outer diameter of 1.9 cm, and a thickness of about 0.6 cm. A 110-turn pick up coil is wound around the CAB toroid. A Stycast 1266 epoxy blank of approximately the same size is then epoxied to the CAB. In order to supply the constant magnetic field for the CAB, approximately 1000 turns of superconducting wire are wound around the toroid. The magnet is

intended to run in a persistent current mode. The thermometer is then placed in a superconducting can for shielding. Figure 2 shows the three different types of PSTs.

Experimental Cell

The measurements will be conducted within the experimental cell illustrated in Figure 3. Sidewall platforms 3 and 2, located 253 μm and 7 mm from the warmer endplate respectively, are used to measure the temperature profile as the interface is positioned at several locations very close to each ring. Close to criticality, measurements taken with platform 3 are affected by the nearby cell endplate while measurements taken with platform 2 are not. Platform 1, located about 14 mm from the warmer boundary, is used to reference and control the superfluid-phase temperature, and to check for any thermal gradients in the superfluid at the larger values of Q.

The insulating sidewalls of the cell are constructed of aluminum alloy 5456 with a measured thermal conductivity of 0.020 W/cm·K at 2.2 K. The isothermal cell endplates and the thermometry stages located along the cell's length are made of ultra-pure (>99.999%) aluminum which is expected to have a thermal conductivity of about 80 W/cm·K [22]. This all-aluminum cell construction provides advantages over conventional cell designs. The cell is constructed by e-beam welded joints, making it robust to large accelerations and to repeated thermal cycling. In addition, the all-aluminum construction has only about one-third of the total cosmic ray absorption cross-section per unit volume than that of a copper and steel cell construction, resulting in low parasitic heating from cosmic ray absorption once the apparatus is in orbit.

Each thermometry stage is constructed by machining two circular rings with a taper to produce a sharp edge on the inner diameter. Each ring is thermally attached to its respective high-resolution thermometer through a >99.999% pure, 1 mm diameter, aluminum wire which is threaded into a hole in the platform and welded in place. Following the e-beam weld of the platform ring to a groove machined into the sidewall, detailed optical studies and an electron microprobe analysis of the weld were performed on a separate test weld, demonstrating excellent joining.

The flight instrument cell will resemble, with a few modifications, the cell described previously. In order to obtain detailed measurements of the non-ohmic thermal conductivity, two thermometers will be

located within 200 μm of each other near the cooler endplate of the cell. A third thermometer will be located about 5 mm from the cooler endplate in order to detect small gradients in the superfluid phase. Although the He I - He II interface, stabilized by the heat flux rather than by gravity, is predicted [4] to exist while in Earth orbit, the flight instrument must be designed to function well if this is not the case. The flight instrument will use the cold endplate as platform 1 with an attached PST. If the interface does not exist while in Earth orbit, then this configuration will ensure that the cell's thermal control loop functions well when normal fluid helium completely fills the cell. Although this configuration will experience the adverse effects of the cell endplate's Kapitza resistance between the regulated endplate and the liquid helium [12,13,14], at the low heat flux levels intended for this experiment, the Kapitza resistance will be separately measured and the bulk temperature can easily be determined.

Cryogenic Valve

A cryogenic valve (Figure 4) is installed in the cell fill line at the radiation shield stage. The valve is hydraulic, using helium as a working fluid [25]. Prior to data collection, the valve is closed and the portion of the cell fill line which connects to room temperature is evacuated. This procedure isolates the cell from pressure variations due to thermal fluctuations and acoustic noise, which would otherwise propagate down to the cell from warmer regions. The use of a preloaded spring makes the cryogenic valve normally-closed. The parasitic heat capacity and thermal conductance of the valve can be greatly reduced by pumping out the hydraulic volume and the valve actuating line before data collection. For space flight, having both the cell fill line and the valve actuating line evacuated before launch provides a measure of security against any possible venting of helium into the guard vacuum. Also, because the cryogenic valve is launched in the closed position, it can more easily withstand launch loads. The version of the cryogenic valve used in the ground experiment permits rapid replacement of the needle and seat by remaking 2 indium O-ring seals; no soldering is required. The ease of rapid replacement permits us to evaluate different needle/seat materials and geometries. Our experience with the ground experiment cryogenic valve is guiding development of a smaller version with a permanent needle and seat. The smaller valve will mount on the same thermal platform as the experimental cell. Mounting the valve on the cell's

thermal isolation platform will eliminate the superfluid thermal link between the cell and the radiation shield stage when the cell fill line is evacuated.

IV. EXPERIMENTAL PROCEDURES

The coarse temperature regulation in the ground-based system is accomplished by feeding the out-of-balance signal from a GRT bridge to a Linear Research LR-130 proportional-integral-differential (PID) temperature controller. The LR-130 in turn provides current to a 5 kΩ resistive heater which is mounted on the stage to be regulated. This technique allows microkelvin regulation in a one Hertz bandwidth. The thermometry bridge consists of a resistive leg, composed of the GRT and a reference resistor located down in the cryostat, and an inductive leg at room temperature. The inductive part, a Gertsch 6-digit ratio transformer, is tuned until it balances the resistive half of the bridge. The out-of-balance signal is detected by a PAR 124A lock-in amplifier which also provides the bridge excitation voltage. This voltage is kept to less than 5 mV across the bridge to minimize self heating of the GRTs. Higher resolution temperature control is achieved by using the signal from a paramagnetic salt thermometer to drive a heater either via the same LR-130 as above, or a computer generated PID signal. Controlling the temperature with the PST system will allow sub-nanokelvin regulation.

The copper ammonium bromide salt thermometer's signal is detected by a Quantum Design SQUID magnetometer. The RF SQUID's signal is first amplified by a Quantum Design model 2000 preamplifier located close to the top of the cryostat and then sent to a model 2010 controller. A custom built flux counter computer board is used to increase the dynamic range of the SQUID controller. This board, based on a design of Professor John Lipa's group at Stanford University, was supplied to the project by the Jet Propulsion Laboratory. The flux counter board provides all reset signals to the SQUIDs and keeps track of how many resets have been sent. Software then accesses each flux count stored on the board which, when combined with its corresponding analog signal from the SQUID controller, represents a relative temperature with sub-nanokelvin resolution. The analog portion of the signal is digitized by a National Instruments 16-bit data acquisition board.

The magnetic field used to charge the PSTs is provided by a 2400-turn superconducting magnet wound around the tail section of the vacuum can. Typical charging fields of about 300-1000 Gauss are used. Once the field is applied, the PST shields are cooled through the superconducting transition temperature, and the external field is turned off. The magnet current leads are then withdrawn from the dewar to lessen boil off.

Data are obtained in the experimental cell by following procedures used previously in a similar experiment performed by Duncan, Ahlers, and Steinberg [11]. A constant heat flux is applied by the heater at the bottom of the cell and the temperature of the cell is controlled by the PST attached to thermometer platform 1 (top ring of the cell) and a heater located at the top of the cell. The temperature at the top of the cell is slowly ramped up toward the normal fluid transition. A ramp rate of a few nanokelvin per second has been achieved. The temperatures of the other two sidewall thermometers (platforms 2 and 3) are monitored until the He I - He II interface has passed platform 2. Measurements will be performed for heat fluxes in the range of 4 nW/cm^2 to 3 $\mu W/cm^2$ providing overlap to the data of Liu and Ahlers [18].

V. THERMAL MODELING

Thermal Model: Probe

Figure 5 displays the thermal model which has been developed to predict the steady-state thermal profile throughout the cryostat during data taking. This thermal model is useful for design and engineering applications, such as the prediction that the cell and PST stage could be raised to above 10 K to recharge the PST flux tubes without disrupting the 1 K refrigerator operation. This prediction was confirmed experimentally.

Assume data is being taken with the thermometer attached to the lower cell ring, which is designated as node 8 in the thermal model. The nylon base, which provides structural support for the cell and PSTs, allows a thermal conductance between this stage and the PST attached to the shield, node 4 in the thermal model. Notice that this heat conduction may be countered by adjusting the temperature of, and hence the heat leak from, the SQUID stage (node 2). This adjustment permits a heat balance at the sidewall thermometer stage, node 8, which is being used in the data taking. Hence, data may be taken

without systematic errors associated with stray heating or cooling from the thermometry stage. Once in Earth orbit, this adjustment of the SQUID stage temperature will allow for compensation of cosmic-ray heating of the sidewall platform used in data acquisition. This heating may vary throughout the orbit, and certainly will vary with any altitude or attitude changes throughout the mission. Typically, the variation in the radial heat flux from the cell sidewall platform is about 2 nW per 1 mK change in the SQUID stage temperature, with the nulling SQUID stage temperature set at about 2.45 K. The conductances of this thermal model are updated as more data are obtained. This thermal model also allows the impact of different materials selections to be evaluated before the flight instrument is developed.

Thermal Model: Experimental Cell

The thermal performance of the experimental cell has been simulated to optimize the sidewall design, and to investigate the cell's ability to resolve the subtle thermal profiles associated with the nonlinear region very near the interface. In all the thermal simulations discussed here, the normal fluid helium bulk thermal conductivity λ is approximated [23] as $\lambda(t,Q) = [\lambda^{-4}(t,0) + \lambda^{-4}(0,Q)]^{-1/4}$, where the zero-$Q$ thermal conductivity is approximated [16] as $\lambda(t,0) = (122.2 + 7.05\ t^{-0.48})$ μW/cm·K and the $t = 0$ limit of the thermal conductivity is taken as its theoretical value [9] of $\lambda(0,Q) = 27{,}400 \cdot Q^{-0.31}$ μW/cm K where Q is in units of μW/cm^2. In the equations above, the reduced temperature is defined relative to $T_\lambda(Q=0)$. For $T < T_\lambda(Q=0)$, the superfluid phase, the helium is forced isothermal by selecting λ(superfluid) = 10,000 W/cm·K. In these simulations the thermal conductivity of the aluminum alloy is taken to be 0.01 W/cm·K and the conductivity of the >99.999% pure aluminum is taken to be 100 W/cm K. The thermal boundary resistance, R_K, between all metal surfaces and the liquid helium is taken to be constant at 0.4 cm^{2}K/W. In these simulations, the He I - He II interface is forced to remain at some height, δ, above the sidewall thermometer platform. The helium sample is taken to be isobaric, as in Earth orbit. A simulation of the thermal profile near the sidewall platform ring is displayed in Figure 6. Here the He I - He II interface is located at $\delta = 50$ μm above the platform ring and normal fluid exists at the position of the platform. A constant heat flux $Q = 0.1$ μW/cm^2 flows through the cell from the bottom to the top. Notice that the radial thermal gradient in the cell is large within about 1 mm of the sidewall. The temperature read by the sidewall platform ring differs from the helium temperature near the center ($r = 0$) of the cell. The

helium temperature near the center of the cell, where no radial temperature variation is noticed, is taken to be the true bulk helium temperature since it shows no sensitivity to the measurement apparatus at the sidewall located at $r = 8.35$ mm. The difference between the actual height of the sidewall thermometer and the position of the temperature isotherm that it measures, Δ, is determined graphically as displayed in Figure 6. For a radial heat flux of zero, Δ is zero. For a given Q, the variation of Δ with δ is weak and readily correctable, making the ultimate data analysis in this experiment possible and not limited by these thermal offsets. Although virtually no heat is generated or absorbed in the thermometry platforms, the abrupt change in the sidewall's effective thermal conductivity in the vicinity of the platform creates a radial component of the heat flux which perturbs the otherwise purely axial heat flux through the cell. This radial heat flux integrated over the entire cell must equal zero since no sources or sinks are present on the platforms. The effect of the thermometry platform's shape, depth of penetration, and proximity to an endplate has been simulated and reported previously [24].

Table 1 displays the variation of Δ with δ. Notice that Δ is primarily a function of Q, and that it varies little with δ, and hence with the distance from criticality. The corrections for the radial thermal gradient primarily depend on Q, and not on the reduced temperature. Experimentally, the superfluid temperature, controlled by a servo loop, is varied so as to position the interface near one of the sidewall thermometry platforms while a constant heat flux passes through the interface. Therefore, only small corrections for the variation of Δ with δ, and hence with the superfluid temperature, need be applied as the data are taken.

Cosmic Ray Heating

Cosmic rays and trapped ions in the South Atlantic Anomaly (SAA) act both on the PSTs and on the experimental cell. LPE carried charged particle monitors that permitted the analysis of the effects of these ionizing radiations on the calorimetric data [20,26,27]. The most significant effect was the increase of noise levels on the PSTs by nearly a factor five over those observed on the ground [20]; this noise increase led to reduced resolution in the temperature measurements. Some of this increase resulted from the unhappy circumstance that the cosmic ray events occurred at about the same rate (1-3 per second) as the PST signals were sampled (1 Hz), which was near the thermal relaxation rates of the PSTs. The noise

increase can be reduced to an insignificant level if two improvements are made [26]; improve the thermal contact of the PSTs to the helium sample to reduce the thermal relaxation time and increase the sample rate on the PSTs. Both of these measures are planned for the low temperature microgravity flight of CHeX, where the noise levels in orbit are not expected to be significantly higher than on the ground [28]. The second effect of the ionizing radiation is heating of the helium sample. On LPE the ~350 gram calorimeter was heated about 0.27-0.8 nW away from the SAA, and 5 nW in the SAA.

DYNAMX requires the same high resolution of its PSTs as the other flight experiments to get the best temperature data. Therefore, DYNAMX will employ the same improvements that are being applied to CHeX. DYNAMX will go further by using high-conductivity aluminum in the thermal links of the PSTs to the experimental cell. The thermal conductivity of this aluminum is expected to outperform the copper used in LPE and CHeX. The lower density of the aluminum will also lead to less heating from cosmic ray hits on the PSTs. These measures should lead to sub-nanokelvin temperature resolution by the PSTs while in orbit. The DYNAMX flight cell is expected to have about one-tenth the mass of the LPE calorimeter, so, with the reduced liquid helium sample volume, the radiation heating will result in a warming of the sample and cell approximately equal to that seen in the LPE mission. However, since DYNAMX is applying heat currents for the experiment and for temperature control, the radiation heat inputs will affect DYNAMX less than they did LPE. Very little of the cell mass is located at the warm end of the DYNAMX cell, so radiation heating will be on the order of picowatts there. Most (~95%) of the DYNAMX cell mass is at the cold end, where the temperature is controlled by a servo loop that applies about 50 microwatts to maintain the temperature. A few nanowatts of radiation heating will have little effect at this location. The SAA passages will cause significant heating only for the lowest, approximately 50 pW, heat currents applied to the warm end of the cell. With careful planning of the experiment, the low heat current data can be obtained in orbits which do not encounter the SAA.

ACKNOWLEDGMENTS

We gratefully acknowledge assistance from the Low Temperature Physics Group of the Jet Propulsion Laboratory. We would also like to thank Steven McCready for his useful comments. This work has been funded through the Flight Program of the Microgravity Science and Applications Division of NASA, and through the U.S. Department of Energy under Contract No. DE-AC04-~~76DP00789~~ 94AL85000.

REFERENCES

[1] J. A. Lipa, B. Leslie, and T. Wallstrom, Physica 107B: 331 (1981).

[2] A. Onuki, J. Low Temp. Phys. 50: 433 (1983); 55: 309 (1984), and references therein.

[3] Available from Helium Operations, Bureau of Mines, Department of the Interior, 801 S. Fillmore, #500, Amarillo, Texas 79101-3545.

[4] P. C. Hendry and P. V. E. McClintock, Cryogenics 25: 526 (1985).

[5] V. L. Ginzburg and A. A. Sobyanin, J. Low Temp. Phys. 49: 507 (1982).

[6] G. Ahlers, Phys. Rev. 171: 275 (1968).

[7] Lambda Point Experiment (LPE); Principal Investigator: J. Lipa, Stanford University.

[8] Confined Helium Experiment (CHeX); Principal Investigator: J. Lipa, Stanford University.

[9] R. Haussmann and V. Dohm, Phys. Rev. Lett. 67: 3404 (1991); Z. Phys. B87: 229 (1992).

[10] R. Haussmann and V. Dohm, Phys. Rev. B 46: 6361 (1992).

[11] R. Duncan, G. Ahlers, and V. Steinberg, Phys. Rev. Lett. 60: 1522 (1988).

[12] R. Duncan, G. Ahlers, and V. Steinberg, Phys. Rev. Lett. 58: 337 (1987); R. Duncan and G. Ahlers, Jpn. J. Appl. Phys. [Suppl.] 26-3: 363 (1987); Phys. Rev. B 43: 7707 (1991).

[13] M. Dingus, F. Zhong, and H. Meyer, J. Low Temp. Phys. 65: 185 (1986); F. Zhong, J. Tuttle, and H. Meyer, J. Low Temp. Phys. 79: 9 (1990); D. Murphy and H. Meyer, unpublished.

[14] T. C. P. Chui, Q. Li, J. A. Lipa, Jpn. J. Appl. Phys. [Suppl.] 26-3: 371 (1987); Q. Li, T. C. P. Chui, and J. A. Lipa, Bull. Am. Phys. Soc. 33: 1373 (1988).

[15] D. Frank, and V. Dohm, Phys. Rev. Lett. 62: 1864 (1989); Z. Phys. B84: 443 (1991).

[16] G. Ahlers and R. V. Duncan, Phys. Rev. Lett. 61: 846 (1988).

[17] Q. Li, Ph.D. Thesis, Stanford University (1990), unpublished.

[18] F-C. Liu and G. Ahlers, Physica B 194-196: 597 (1994); and unpublished.

[19] R. P. Behringer, Rev. Mod. Phys. 57: 657 (1985).

[20] J. A. Lipa, "Lambda Point Flight Experiment Final Report," document LPE 192.STR, (Stanford University, 1994).

[21] R. Duncan, Ph.D. Thesis, University of California at Santa Barbara (1988), unpublished.

[22] Y. S. Touloukian, R. W. Powell, C. Y. Ho, and P. G. Klemens, Thermophysical Properties of Matter, Volume 1, "Thermal Conductivity : Metallic Elements and Alloys" (IFI/Plenum, New York, 1970).

[23] F-C. Liu and G. Ahlers, unpublished.

[24] R. Duncan, R. Akau, S. Gianoulakis, U. Israelsson, and T. Chui, Physica B 194-196: 603 (1994); and unpublished.

[25] Pat R. Roach, J. B. Ketterson, and M. Kuchnir, Rev. Sci. Inst. 43: 898 (1972).

[26] D. R. Swanson, J. A. Nissen, T. C. P. Chui, P. R. Williamson and J. A. Lipa, Physica B 194-196: 25 (1994).

[27] P. Roger Williamson, "Charged particle monitor measurements on the Lambda Point Experiment USMP-1/STS-52," Stanford Technical Report LPE 193.STR (1994).

[28] P. Roger Williamson, private communication.

DISCLAIMER

FIGURE CAPTIONS

Table 1: Variation of Δ with δ and heat flux Q.

Figure 1: Schematic of the low temperature probe.

Figure 2: Photograph of the three types of paramagnetic salt thermometers. From top to bottom: toroidal PST with its shield, packed powder PST, and PST using crystalline CAB and a sapphire cylinder.

Figure 3: Experimental cell.

Figure 4: Schematic cross-sectional view of cryogenic valve. The lower outlet is connected to the cell. Actuation outlet and second cell fill line outlet are superimposed in this view. The lower part of the valve is deliberately oversized to ease replacement of needle and seat.

Figure 5: Schematic representation of the thermal model. Each number represents a thermal node in the model. Q2, Q3, etc. represent the heat applied to a given node.

Figure 6: Simulation of the thermal profile near a sidewall platform. Each band represents a change of approximately 10 nanokelvin.

$\delta(\mu m)$	$\Delta(\mu m)$, $Q = 0.1\mu W/cm^2$	$\Delta(\mu m)$, $Q = 1.0\mu W/cm^2$
0	170 ± 10	300 ± 10
50	160	290
100	135	270
500	145	270

Table 1

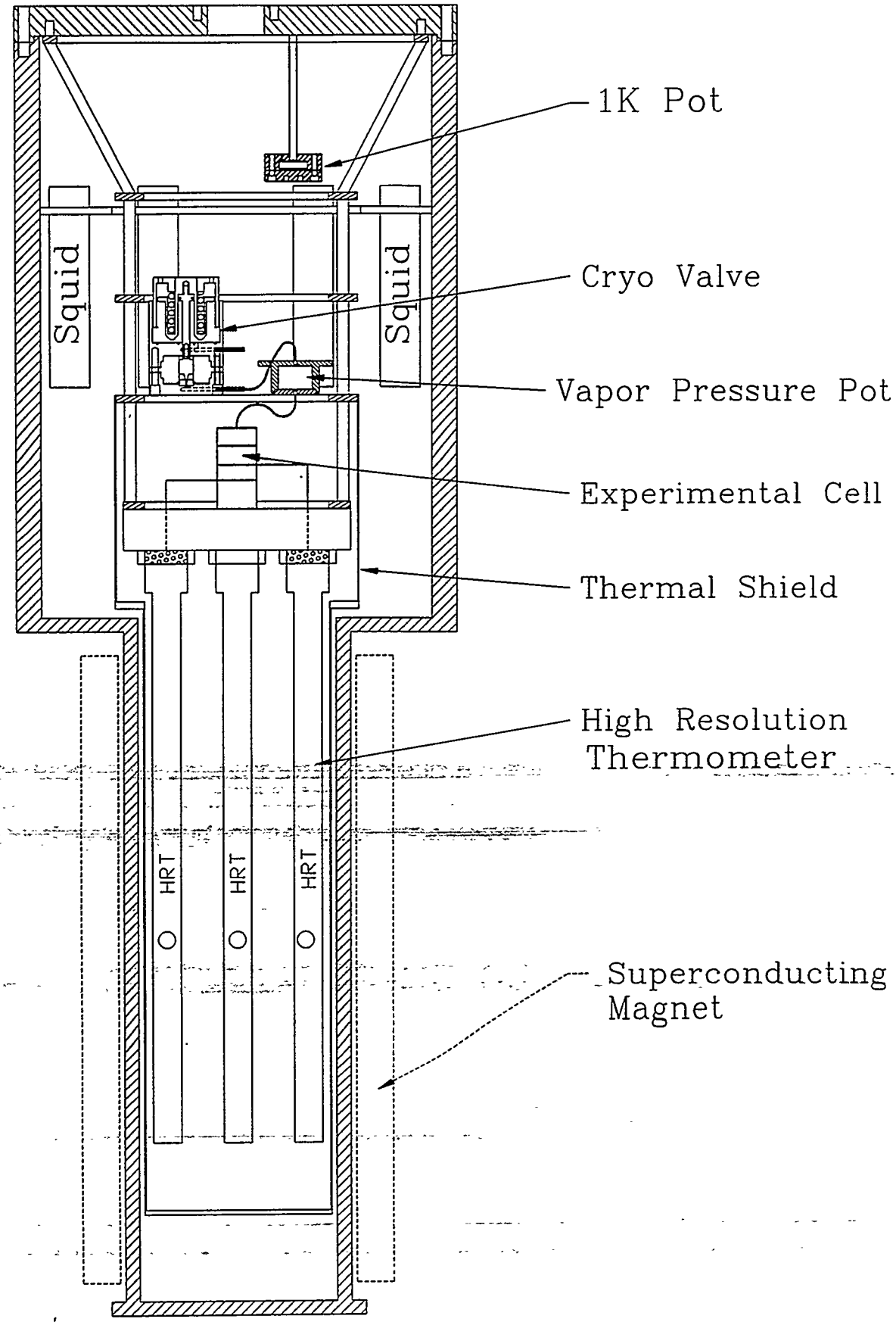
1K Pot
Squid
Squid
Cryo Valve
Vapor Pressure Pot
Experimental Cell
Thermal Shield
High Resolution Thermometer
HRT
HRT
HRT
Superconducting Magnet

Figure 1

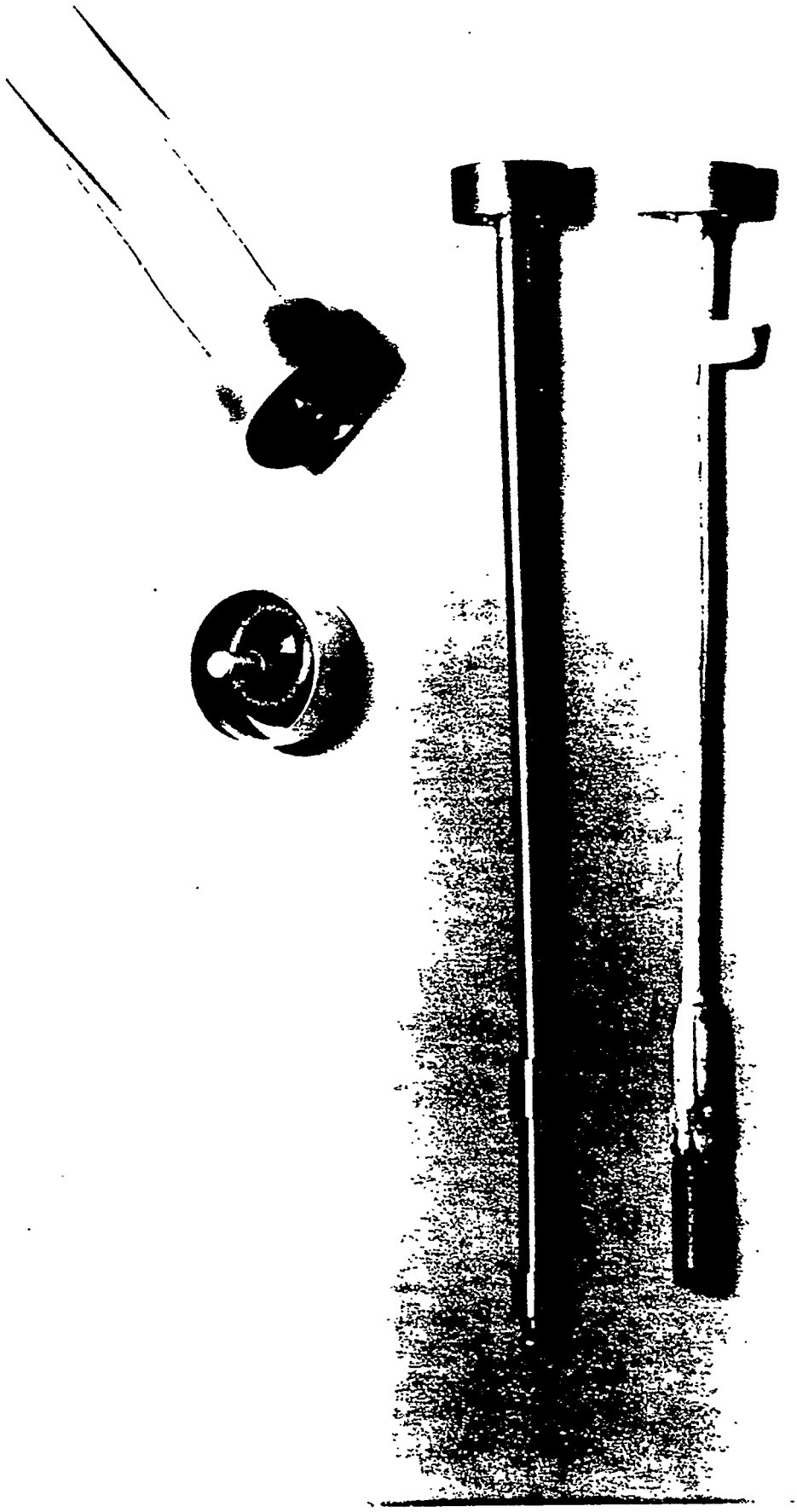

Figure 2

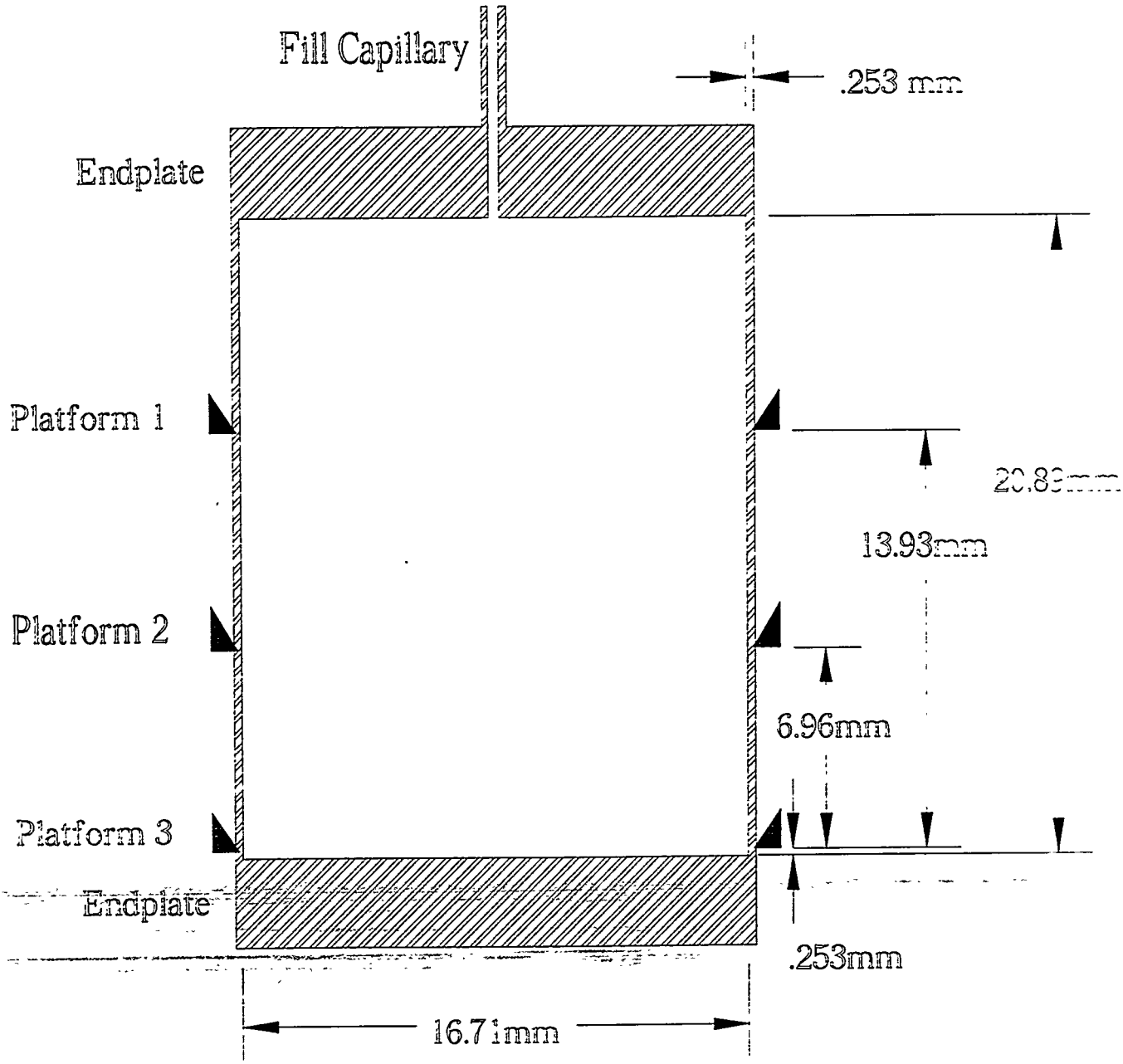
Fill Capillary
.253 mm
Endplate
Platform 1
20.83mm
13.93mm
Platform 2
6.96mm
Platform 3
Endplate
.253mm
16.71mm

Figure 3

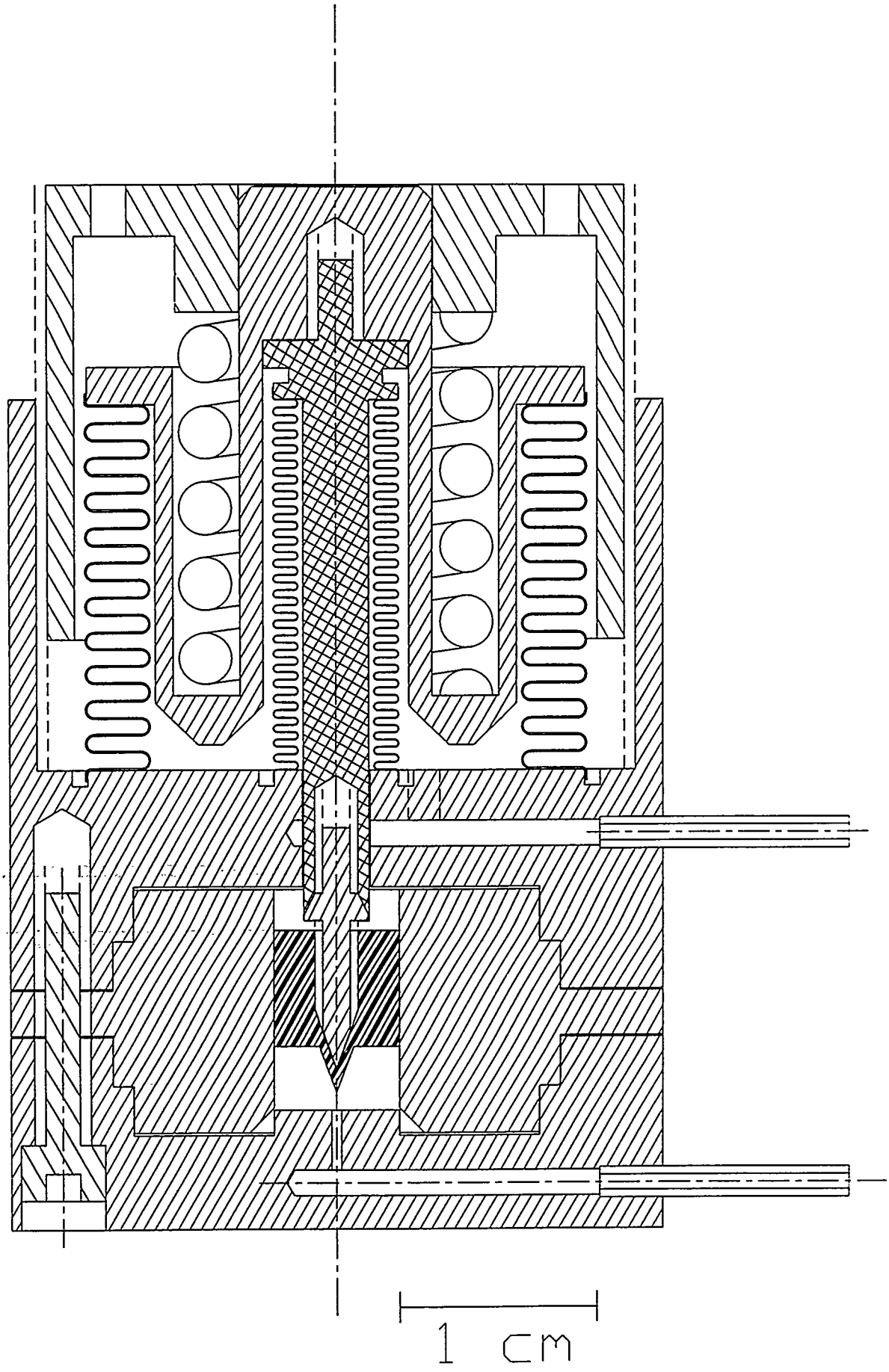
1 cm

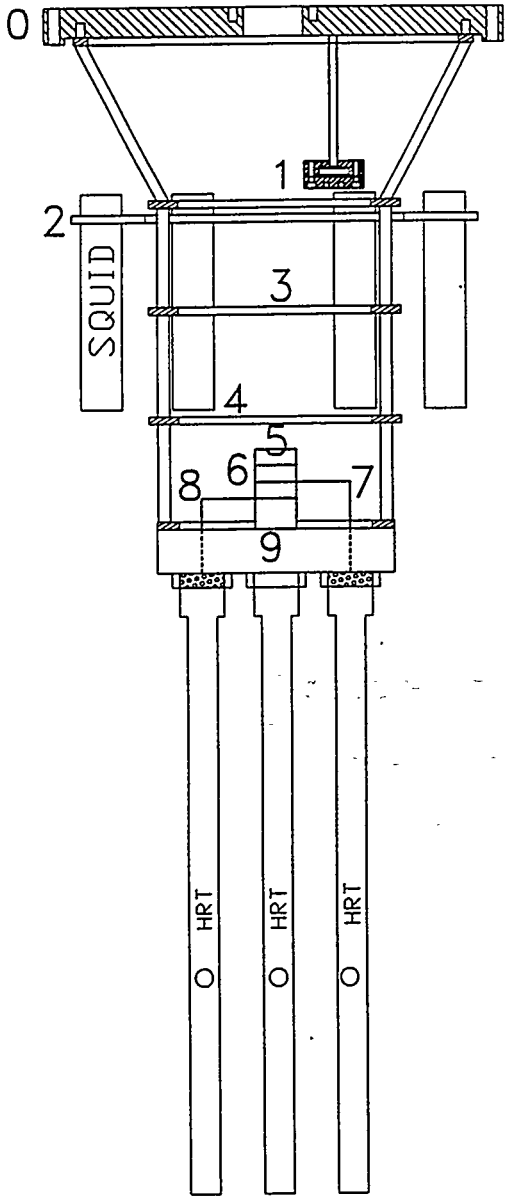
0
1
2
SQUID
3
4
5
6
7
8
9
HRT
HRT
HRT

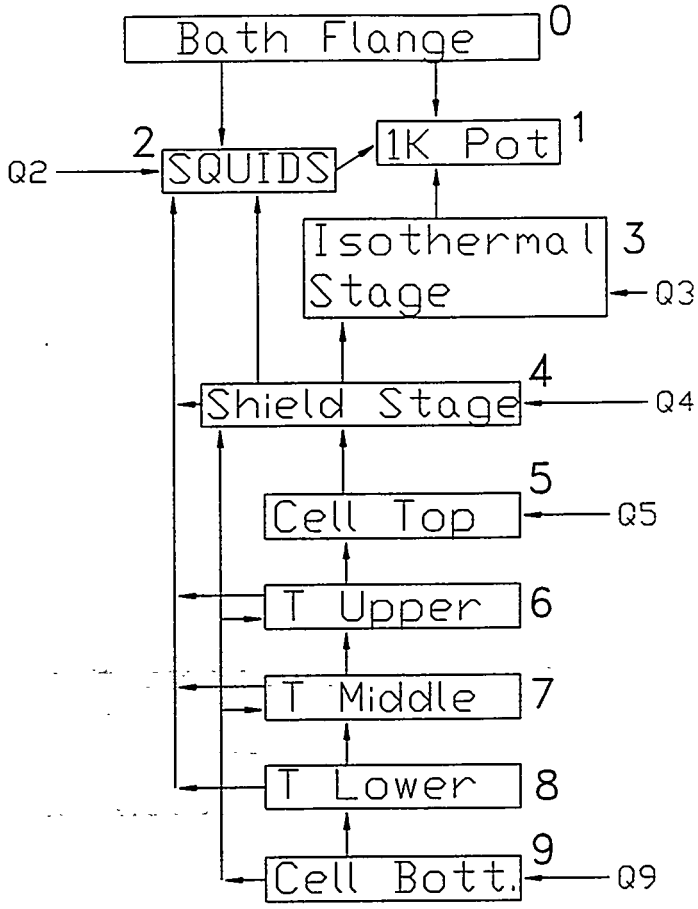
Bath Flange
0
1K Pot
1
Q2
2
SQUIDS
Isothermal Stage
3
Q3
Shield Stage
4
Q4
Cell Top
5
Q5
T Upper
6
T Middle
7
T Lower
8
Cell Bott.
9
Q9

Figure 5

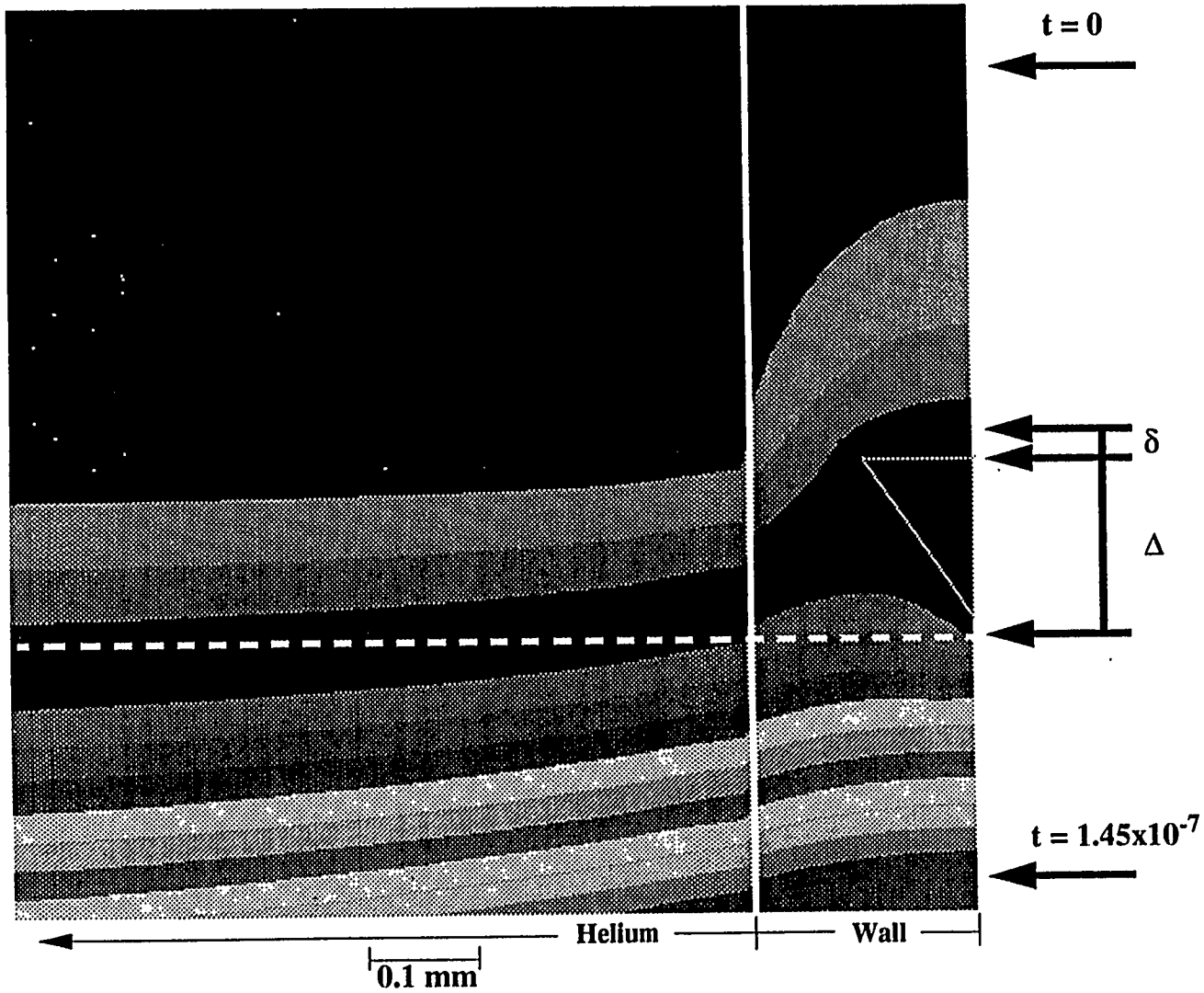
t = 0
δ
Δ
t = 1.45x10^-7
Helium
Wall
0.1 mm